Available online at www.sciencedirect.com

SciVerse ScienceDirect

Procedia Engineering 58 (2013) 624 – 633

Procedia Engineering

www.elsevier.com/locate/procedia

The 12th Hypervelocity Impact Symposium

Time-Resolved Emission Spectroscopy of Impact Plasma

Dominic Heunoske[a]*, Martin Schimmerohn[a], Jens Osterholz[a] and Frank Schäfer[a]

[a]*Fraunhofer EMI, Eckerstraße 4, 79104 Freiburg, Germany*

Abstract

One phenomenon observed at hypervelocity impacts (HVI) is the generation of plasma with a very short lifetime of a few microseconds. Due to this short lifetime, characteristic plasma parameters such as the electron density and the electron temperature of the expanding plasma were not investigated thoroughly in the past. This paper will present a method to measure these parameters with a time-resolution of 500 ns for the full period of impact plasma expansion and discuss results gained in impact experiments.

At the Fraunhofer EMI, impact experiments on solar panels were performed using a two-stage light-gas gun to accelerate aluminum spheres with a diameter of a few millimeters up to a speed of 8 km/s. A measurement system consisting of a spectrograph and a streak camera was applied for time-resolved spectroscopy of the impact plasma.

To derive plasma properties, the recorded streak image was evaluated using different methods for different expansion states of the plasma cloud. The spectra show strong self-absorption lines in the first microseconds of expansion. In the present work, these features are explained by the electron density and temperature gradient in the plasma. For the determination of electron temperature and density, a one-dimensional radiative transfer model was adapted to the measured spectra. After 2 µs of expansion, the plasma is optically thin and emission lines can be observed. For this expansion state, the electron temperature was determined by the ratio of line to continuum radiation, whereas the electron density was determined through the line broadening due to the Stark effect.

Using these methods, it was found that the electron temperature decreases in the first 3 µs of propagation from 45,000 K to 2,000 K in the experiments performed. The electron density decreases from 10^{19} cm^{-3} to 10^{17} cm^{-3}.

Selection and peer-review under responsibility of the Hypervelocity Impact Society

Keywords: hypervelocity impact plasma, time-resolved spectroscopy, electron temperature, electron density

Nomenclature

A	Einstein coefficient spontaneous emission	B	Einstein coefficient stimulated emission
c	speed of light	C	summarized constants
P	radiated power	d	Stark shift parameter
f	frequency	g	degeneracy
G	Gaunt-factor	h	Planck constant
I	intensity	k	Boltzmann-factor
n	number density	U	partition function
v	projectile speed	w	Stark width parameter
x	location	Y	line profile function

Greek symbols

$\grave{o}$	emission coefficient	κ	absorption coefficient
λ	wavelength	$\Delta\lambda$	line width

* Corresponding author. Tel.:+49 761 2714 578.
E-mail address: Dominic.Heunoske@emi.fraunhofer.de

Selection and peer-review under responsibility of the Hypervelocity Impact Society
doi:10.1016/j.proeng.2013.05.072

ν	frequency	ξ	Biberman-factor
σ	distribution parameter		
Subscripts			
0	unperturbed	*1*	lower state
2	upper state	*c*	continuum
d	shifted	*e*	electron
fb	free-bound	*ff*	free-free
l	line		

1. Introduction

The impact plasma is created by the impact of particles with speeds of at least 2 km/s. Due to the high speeds, a shock wave spreads through the target and projectile. This leads to sudden shock wave compaction with pressures in the range of 100 GPa and temperatures in the range of 10^5 K. When the shock wave releases, the material evaporates and escapes at an angle which depends on the projectile velocity [1], the projectile shape and on other factors. The vaporized material is so hot that it is partially ionized and is therefore referred to as impact plasma. Due to its very short lifetime and high intensity the emitted light is also known as impact flash. The flash produced by the impact of the SMART-1 spacecraft on the Moon on 3rd September 2006, could be recorded from the Earth [2].

The phenomenon of impact flash has already been known for long. In 1959, initial studies were carried out by Clark [3]. The emitted light was explained by collisions of the ejecta with the ambient atmosphere. In the following years, several studies were made to explore the phenomenon of impact flash. In 1976, Eichorn performed impact experiments with a Van De Graf dust accelerator [4]. Particles with a mass from 10^{-9} g to 10^{-16} g were accelerated up to 35 km/s. Eichorn discovered a correlation between the radiated light intensity and the projectile speed and mass. From the spectral distribution of the emitted light, the temperature of the radiating material was estimated to be between 2,500 K and 5,000 K.

Goetting carried out HVI experiments with aluminum and copper [5]. Projectiles with a diameter of 2.5 mm were accelerated to up to 4.8 km/s. The light of the impact flash passed through a spectrograph and was recorded by an image converter camera. The spectra showed a broadband continuum emission at the beginning of the impact flash that changed in a few microseconds to a line spectrum. The recorded lines stem from both the target and the projectile material. Goetting concluded that both target and projectile evaporate partially during impact. From spectral lines of ionized aluminum, it could be shown that the metal vapor is ionized to a considerable extent and the name impact plasma is therefore correctly applied. By comparing the recorded spectra with calculations that were carried out by Harwell [6], Goetting estimated that the temperature of the impact plasma is at about 10,000 K.

In recent years, a number of spectral measurements were performed on impact plasma. In 2003, Sugita conducted measurements with copper projectiles accelerated up to 5.5 km/s; the target was made of dolomite. The power, radiated from the plasma, was integrated over the visible spectral range. It was found, that the radiated power is a function of projectile velocity ($P \propto v^5$) and a theoretical model to describe this function was developed [7]. Sugita and Schulz also determined the temperature of impact plasma inferred from Boltzmann distribution of the emitted light from 4000 K to 6000 K [8].

Lawrence [9] and Rheinhart [10] carried out experiments in 2006 with two- and three-stage light-gas guns as well as the Z-machine. Aluminum projectiles were accelerated on aluminum and quartz targets. With the Z-machine, projectiles with a diameter of 0.85 mm were accelerated to up to 25 km/s. With the light-gas guns, spheres and aluminum flyer plates made of titanium or tantalum were accelerated up to 11 km/s. The resulting plasma was studied by time-resolved spectroscopy. The authors observed continuum radiation, line emission and absorption lines.

Tsemblis [11] performed experiments with a 2 MV van de Graaff accelerator. Iron dust particles with a diameter of up to 0.63 µm were accelerated on soda-lime glass at velocities of 5 km/s – 20 km/s. The light flash temperature was determined by comparing the emitted spectra with blackbody radiation. Tsembelis found an average temperature of 2600 K independent of the projectile speed.

A time-resolved determination of important plasma parameters such as e.g. electron density and temperature, however, hasn't been done yet for impact plasmas. In contrast, the time resolved measurement of plasma parameters has been widely applied for laser produced plasmas using plasma spectroscopy. In general, the derivation of plasma parameters from the spectra emitted by laser produced plasmas or impact plasmas requires models that take into account for transient effects and the expansion of the plasma during the emission [12]. In the present work, we have adapted a model developed by Sakka that was originally developed for laser produced plasmas for the analysis of spectra emitted from impact plasmas [13].

Sakka examined plasmas that are generated by the short-term exposure of a laser beam onto a solid target. The resulting plasmas show similar phenomena to impact plasma. The lifetime of these laser induced plasmas is in the microsecond range; the spectra reveal the presence of continuum and line emission and the electron density and temperature are similar in magnitude.

In the measured spectra, Sakka observed strong self-absorption in the spectra. The reason for this self-absorption is a temperature gradient in the plasma. In 2002, Sakka developed a model for optically thick plasma. Sakka developed a one-dimensional radiative transfer model to determine the electron density and temperature of the Plasma [13]. In this model, only line emission is taken into account. This model was extended by Pakhal [14] for the continuum component in the spectrum. A similar model will be used in this paper to determine electron density and temperature of impact plasma for the first microsecond of expansion.

In the later expansion, the plasma becomes optically thin and plasma parameter can be determined as it was done by Liu [15]. In this study, the electron temperature was determined from the ratio of line to continuum radiation. The electron density was determined from the line broadening of silicon spectral lines via the Stark effect.

With these methods, the electron density and temperature will be determined in this work with a time-resolution of 500 ns for more than 3 µs of expansion.

2. Theory

In this section, the one-dimensional radiative transfer model will be introduced. Since the radiation emitted and absorbed by plasma depends on electron density and temperature, it is a function of space in an inhomogeneous plasma. This situation is described by the following radiative transfer equation:

$$\frac{dI(\nu,x)}{dx} = \dot{o}(\nu,x) - \kappa(\nu,x)I(\nu,x) \tag{1}$$

Both the emission and absorption coefficient consist of a line and a continuum part. The emission coefficient for line radiation can be calculated by [14]:

$$\dot{o}_l = \left(\frac{h\nu}{4\pi}\right) A_{21} n_2 * Y \tag{2}$$

This kind of radiation is emitted by the transition of an electron from a bound excited to an energetic lower state. At low density, the line width is very small and is a function of the lifetime of the exited state. The absorption coefficient for line radiation is defined as:

$$\kappa_l = \frac{h\nu}{c}\left[B_{12}n_1 - B_{21}n_2\right] * Y \tag{3}$$

In dense plasmas, the line shape is significantly broadened by the interaction of the particles in the plasma with each other. The lifetime of the excited states is reduced by collisions, and therefore the line width is enhanced. In addition, the electric fields generated by adjacent free electrons and ions affect the atomic and ionic energy levels in the plasma environment and result in Stark broadening and a shift of the resonance lines. The width and shift of the spectral line due to the Stark effect is a function of the electron density. A linear approximation yields acceptable result. Line shift and width can be calculated by [13]:

$$\Delta\lambda_{width}(n_e) = w * n_e \tag{4}$$

$$\Delta\lambda_{shift}(n_e) = d * n_e \tag{5}$$

The continuous radiation is emitted by two different processes. The first kind of continuous emission is produced when free electrons are scattered by ions. This kind of radiation is called free-free emission, and the emission coefficient can be calculated:

$$\dot{o}_{ff} = \left(\frac{16\pi e^6}{3c^2\left(6\pi m^3 k\right)^{\frac{1}{2}}}\right)\frac{n_e n_i}{T_e^{1/2}}\left[\mathrm{G} * exp\left(-\frac{h\nu}{k_B T}\right)\right] \tag{6}$$

The other kind of continuous radiation is the free-bound emission. It is emitted when a free electron recombines with an ion in the plasma. The emission coefficient can be calculated as:

$$\dot{o}_{fb} = \left(\frac{16\pi e^6}{3c^2 \left(6\pi m^3 k\right)^{\frac{1}{2}}} \right) \frac{n_e n_i}{T_e^{1/2}} \left[\xi^* \left(1 - exp\left(-\frac{h\nu}{k_B T} \right) \right) \right] \tag{7}$$

For the calculation of the radiative properties in the impact plasma, appropriate assumptions have to be made about the geometry as well as the spatial and temporal distribution of the plasma. Pakhal [11] assumed that the density of the plasma is distributed symmetrically to the impact area and can be described by a Gaussian distribution. The expressions for the population density in the exited and the lower state n_2 und n_1 of the plasma are:

$$n_1(x) = N_{10} * \exp\left(-\frac{x^2}{\sigma_1^2} \right) \tag{8}$$

$$n_2(x) = N_{20} * \exp\left(-\frac{x^2}{\sigma_2^2} \right) \tag{9}$$

With the maximum population at the center of the plasma and the standard deviation, this is given by the propagation of the plasma. The ratio population in the upper and lower state is a function of the temperature and can be estimated from the Boltzmann distribution [14]:

$$\frac{N_{20}}{N_{10}} = \frac{g_2}{g_1} \exp\left(-\frac{h\nu_o}{k_b T} \right) \tag{10}$$

The temperature gradient of the plasma is included in the simulation by the ratio of σ_1/σ_2. For the calculation of the coefficients, the line profile P is required. In the present work, the line shape is approximated by a Lorentz profile:

$$Y(\nu, x) = \frac{1}{\pi} * \frac{\Delta\nu(x)/2}{\left[\frac{\Delta\nu(x)}{2} \right]^2 + \left[\nu - \nu_0 + \Delta\nu_d \right]^2} \tag{11}$$

The width of this line profile is determined by the Stark width and thus depends on the electron density. Also for the electron density, a Gaussian distribution was assumed:

$$n_e(x) = N_e * \exp\left(-\frac{x^2}{\sigma_e^2} \right) \tag{12}$$

3. Experimental setup

The experiments were performed with EMI's Space Light-Gas Gun (SLGG). The SLGG is a two-stage light-gas gun, which is able to accelerate projectiles with a diameter of a few millimeters up to 10 km/s.

The measuring system, which records the spectrum of the impact plasma, consists of several components. These include a collimating lens, an optical fiber, a spectrograph and a streak camera. To record the spectrum, the light of the impact plasma is focused by a collimator to a fiber and then passed into a spectrograph. In the spectrograph, the light is spectrally separated in the horizontal plane. A Czerny-Turner spectrograph with a 1,200 grooves/mm grating and a focal length of 0.3 m was used. The entrance slit was predetermined by the diameter of the fiber (200 µm). With these settings a spectral resolution of 0.48 nm was obtained.

The spectrograph was connected to the streak camera. In the streak camera, the light passing through the input slit is focused onto the photocathode of the streak tube by the input optics. The photocathode converts the light into photo electrons that are accelerated by an electric field onto a phosphor screen. An electro-optical focusing system allows focusing the electrons on the screen. After passing the anode aperture the photo-electrons are deflected by a transversal electric field that increases linearly with time before reaching the phosphor screen. In this way, the input spectra from different points of time are spatially separated on the phosphor screen. The phosphor layer converts the electrons into light that can be observed, via an image intensifier, by a coupled CCD camera. The complete experimental setup and operation mode of the measurement system is shown in Fig. 1.

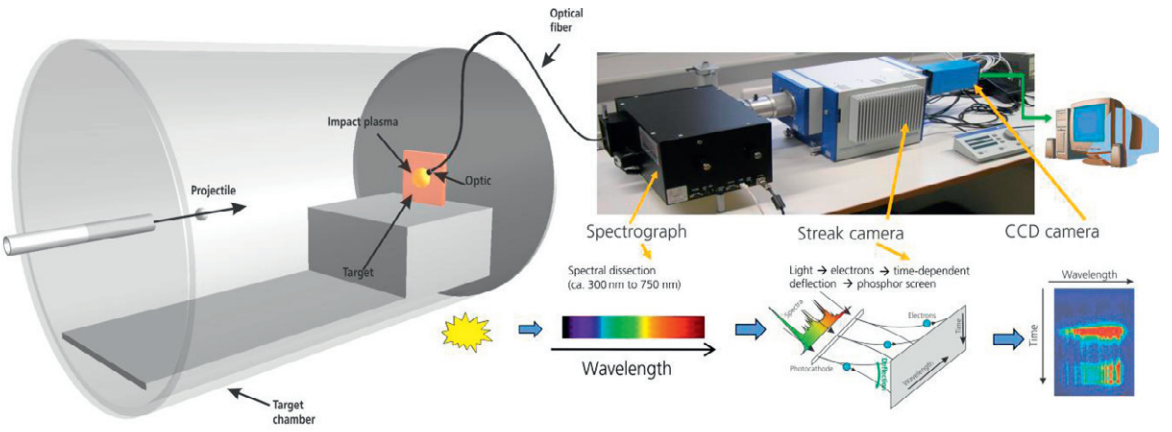

Fig. 1. Experimental setup and operation mode of the measurement system.

4. Experiments and results

The measurement system was used for a study of the European Space Agency (ESA). In this study, impact tests were performed with solar panels, similar to the ones used on satellites. The aim was to evaluate the susceptibility of these modules by the impact of space debris. Particularly, discharges generated by impact plasma were studied.

The impact angle of these experiments was 45° to the shot axis, and the projectiles were made from pure aluminum (Al 99.99%) with a diameter of 1.588 mm. The velocity of the shot that is evaluated in this section was 7.5 km/s. A picture of the target after the shot can be seen in Fig. 2. The pressure in the target chambered was 10^{-4} mbar, thus allowing for neglecting plasma interactions with the residual atmospheres.

The recorded spectrum in Fig. 3 shows the same features as described in the literature. There is continuous emission at the beginning of the expansion. This continuous emission decreases very quickly, and about 1 µs after impact, the spectrum is dominated by line emission. But as can be seen in Fig. 3 a), the spectrum shows strong self-absorption lines. The determination of the plasma parameter electron density and temperature for the different kinds of spectra is described in the next two sections.

4.1.1. Optically thick region

The reason for the self-absorption at the beginning of the plasma expansion is a temperature and density gradient in the plasma. The continuous radiation that is emitted from the center of the plasma is absorbed by cooler atoms in the outer area of the plasma at the wavelengths of the transitions at 394.4 nm and 396.1 nm. For the analysis of the spectra and the deviation of the plasma parameters, both lines are considered.

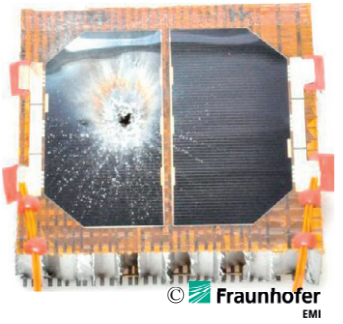

Fig. 2. Photograph of a solar panel target after impact test.

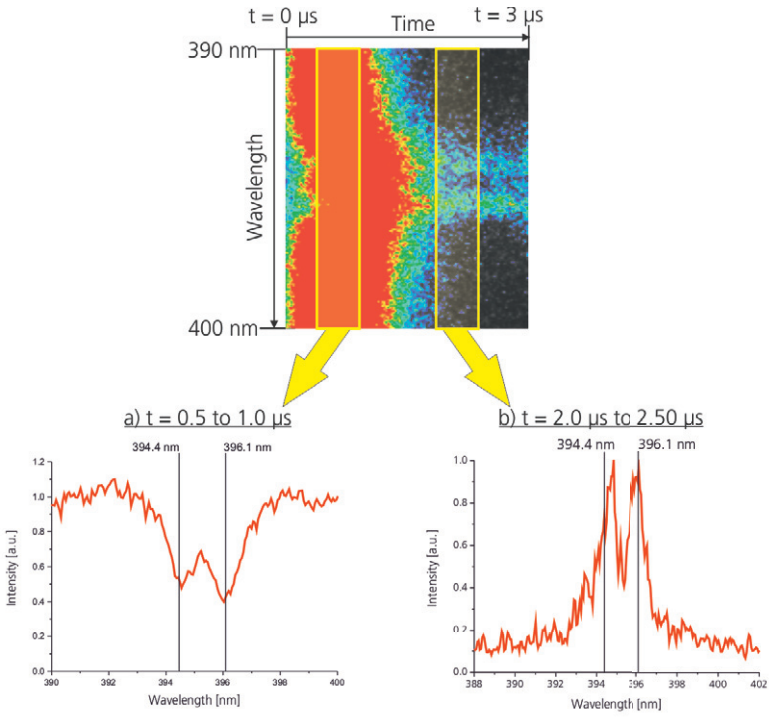

Fig. 3. Time-resolved spectra of an impact test with solar panel target and aluminum projectile. A grating with 1200 grooves/mm was used to record the emission of the $3s^23p^2$-$3s^24s^2$ doublet of neutral aluminum with a wavelength of 394.4 nm and 396.1 nm. The recorded spectra show a) absorbtion lines in the beginning of plasma expansion when the plasma is optically thick and b) emission lines after 2 µs when the plasma becomes optically thin.

For the calculation of the spectrum emitted from the impact plasma, the one dimensional radiative transfer equation (1) has to be solved. To this end, some additional assumptions have been made to reduce the number of parameters in the simulation. The population distribution in the lower states of the two transitions, a = 394.4 nm and b = 396.1 nm, is as follows [13]:

$$\frac{N_{1a}}{N_{1b}} = \frac{g_a}{g_b} \tag{13}$$

From high-speed imaging, the propagation of the plasma during the expansion is known. It is presumed that the electron density decreases till the edge of the plasma to below 5 % of the maximum value. Thus, the distribution parameter of the electron density is equal to a quarter of the visible plasma. The same assumption was made for the distribution of the upper state, which is the same for both transitions.

The parameters that have to be adjusted were σ_1, N_e, N_{1a} and T. The depth of the absorption lines depends on the quotient of σ_1/σ_2. This quotient is equivalent to the temperature gradient in the plasma. The width of the self-absorption lines is dependent on N_e and N_{1a} due to the Stark effect. The temperature mainly affects the shape of spectrum in the regions far away from the wavelengths of the transitions.

Another effect that must be considered when simulating the spectrum is the finite resolution of the spectrograph. The simulated spectrum has to be convolved with the instrument function of the spectrograph in order to compare it with the measured spectrum:

$$I(\nu) = \int_{-\infty}^{\infty} I(\mu) g(\nu - \mu) d\mu \tag{14}$$

As instrument function of the spectrograph, a Lorentz distribution was used with a half-width of $\Delta\lambda = 0.48$ nm. Adapting this model to the measured spectra, it could be shown that the electron density and temperature decrease very fast in the first 1.5 µs of expansion (see Fig. 4 b)). The electron temperature decreased from 45,000 K to 32,000 K and the electron density decreased from $2*10^{19}$ cm^{-3} to $1*10^{19}$ cm^{-3}. Further, it could be observed that the depth of the self-absorption, and therefore

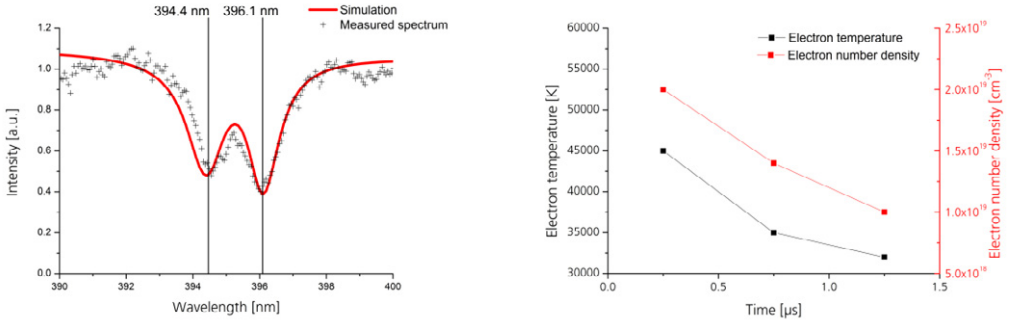

a) b)

Fig 4. Measured spectrum (black symbols) compared with simulation (red line) a) and temporal evolution of electron density and electron temperature in the optically thick region.

the temperature gradient gets weaker and the plasma homogenizes during the expansion. All data used for the simulation is given in Table 1, Appendix A.

4.1.2. Optically thin region

About 1.5 µs after the impact, the spectrum is dominated by line emission. For the remaining period of propagation, methods for optically thin plasma were used to determine plasma parameters. This clause describes the calculation of the spectrum and the derivation of the electron density and temperature in the impact plasma. Similar to the previous paragraph, the sum of two line profiles was fitted to the measured spectra (See Fig. 5). The line shape is mainly determined by the Stark broadening. Therefore a Lorentz distribution was chosen. Doppler broadening, which would lead to Gaussian distribution, has no influence on the line shape at the measured electron temperatures.

Quantum mechanical considerations show that both the width and intensity of the spectral lines must be equal. Therefore, a sum over two Lorentzian distributions is adapted to the spectra. The offset takes into account the intensity of the continuum radiation. The integrated area under the line and the width is assumed to be equal for both emission lines to reduce the free parameters of the fit. Since the resolution of the spectrometer doesn't allow for the measurement of the Stark shift, the line width is used for the determination of the electron density. The latter is related to the width of the emission lines according to Equation (4). However, the width of the instrument function has to be considered. Since there are two Lorentzian profiles, one can easily deduct the width of each other.

$$\Delta\lambda_{width} = \Delta\lambda_{\text{fit}} - \Delta\lambda_{\text{instrument}} \tag{15}$$

From the measured line width, the temporal evolution of the electron density was derived. The result is shown in Fig. 6 b). One can see a significant decrease in the electron density from $9*10^{18}$ cm^{-3} to $2*10^{18}cm^{-3}$ within 2 µs. Due to the expansion of the plasma, this drop seems very plausible.

In Figure 6, the error of the electron density was estimated from the error of the fit over the Gaussian error propagation. In fact, the error might be higher due to the linear approximation of the line width (see Equation (4)). Moreover, the slight electron temperature dependence of the Stark parameter wasn't considered.

In addition to the electron density, the electron temperature of the plasma can be calculated from the parameters of the performed fit. According to Reference [16], the ratio of line to continuum emission is a function of electron temperature and follows as:

$$\frac{\varepsilon_l}{\varepsilon_c}(\lambda) = C\ \frac{A_{21}g_2}{U}\frac{\lambda_c^2}{\lambda_l T_e}\frac{1}{\xi}\exp\left(\frac{E_i - E_2}{kT_e}\right) \tag{16}$$

The ratio $\varepsilon_l/\varepsilon_c$ was calculated from the fit parameters. The temporal evolution of the electron temperature was then calculated according to Equation (16). The result is shown in Fig. 6 a). The electron temperature decreases within 2 µs from 2,100 K to 1,800 K.

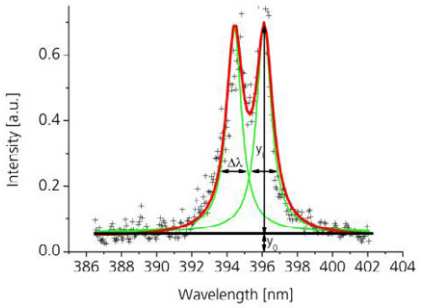

Fig 5. Calculated (red line) and measured (black +) spectrum emitted from the impact plasma. The calculated spectrum is a sum over two single Lorentz distributions (green lines) with maximum y_l over a continuous background y_0 with the line width $\Delta\lambda$.

.

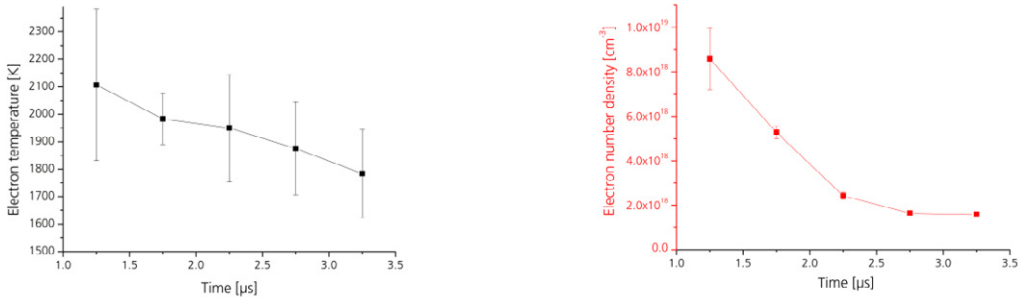

a) b)

Fig 6. Temporal evolution in the optically thin region of the electron temperature a) and the electron density b).

The error of these results is obtained from the errors of the fit. This error is probably too small, since the impact plasma produced from the solar panels contains a large number of chemical elements whereas the model is strictly only valid for pure elements.

Impact experiments with pure aluminum targets, however, provide the same results. Electron temperature determinations by comparing different emission lines, measured at experiments with copper targets, produce electron temperatures and densities in the same order of magnitude.

A necessary condition for the determination of the electron temperatures via the ratio of line to continuum emission is a local thermal equilibrium (LTE) in the plasma. This assumption is valid if [17]:

$$n_e \geq 9*10^{17}\left(\frac{E_{21}}{E_i}\right)^3 * \sqrt{\frac{kT_e}{E_i}}\ [cm^{-3}] \tag{17}$$

This condition is fulfilled by more than two orders of magnitude with the measured results. All data used for the determination of plasma parameter is given in Table 2, Appendix B.

5. Conclusion

For experiments with solar panel targets, the time-resolved determination of the electron density and temperature during the whole period of expansion was successful (Fig. 7). For the initial region of propagation, optically thick plasma with a spatial temperature gradient, which leads to self-absorption lines, was observed. A one-dimensional radiative transfer model was adapted to the measured spectrum. From this adaptation, electron densities and temperatures were obtained. It was found that the electron density drops in the first 1.5 µs of the propagation from $2*10^{19}$ cm^{-3} to $1*10^{19}$ cm^{-3}. The electron temperature decreased from 45,000 K to 32,000 K.

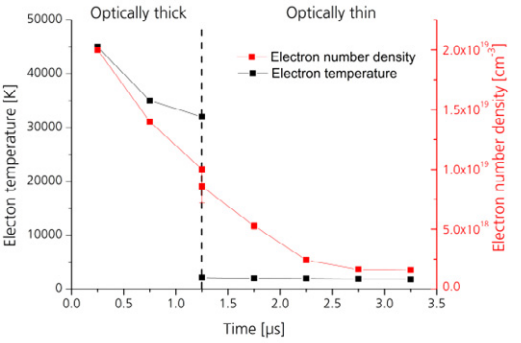

Fig 7. Temporal evolution of electron density and temperature during the whole period of expansion.

For the optically thin region of expansion the electron density was determined over the line broadening caused by the Stark effect. A decrease from $8.6*10^{18}$ cm^{-3} to $2*10^{18}cm^{-3}$ was obtained. During this period, the electron temperature was determined via the ratio of line to continuum radiation and decreases from 2,100 K to 1,790 K.

In the transition region from optically thick to optically thin plasma both evaluation methods were applied to the spectrum. Both methods produce similar electron density, but the obtained electron temperature differs. In this transition region none of the two models fits the characteristic features of the spectrum very well. It is likely that neither method produces very accurate electron temperatures in this transition region.

These results lead to a better characterization of the impact plasma and contribute to measures that may enhance the lifetime of satellites.

Acknowledgements

Parts of the work described in this report were done under European Space Agency contract 22462/09/NL/GLC in support of the German ARTES 5.1 contribution by the German Space Agency.

References

[1] Ang, J., 1990, Impact Flash Jet Initiation Phenomenology. International Journal of Impact Engineering, Volume 10, Issues 1–4, pp. 23–33.
[2] Burchell, M. J., 2010, Robin-Wilians, R., Foing B.H., The SMART-1 lunar impact, Icarus, Volume 207, Issue 1, pp. 28–38.
[3] Clark, J. S., 1959, Kadesh, R. R., Grow, R., Spectral Analysis of the Impact of Ultra Velocity Copper Speres into Copper Targets. Univeristy of Utah, Techn. Report No. OSR-13.
[4] Eichhorn, G., 1976, Analysis of The Hypervelocity Impact Process From Impact Flash Measurements, Plasnet Space Sci., Vol. 24, pp. 771–781.
[5] Götting, G., Das Impact-Leuchten. Dissertation, EMI-Bericht Nr. 2/77, 3.2.1977.
[6] Harwell, K., Reid, J., Hughes, A., 1971, Calculated Equilibrium Composition and Radiation of Metallic Plasmas Produced in Hypervelocity Impakt, Journal of Spacecraft and Rockets, Vol. 8, No. 4., pp. 358–366.
[7] Sugita, S., Schultz, P. H., Hasegawa, S., 2003, Intensities of Atomic Lines and Molecular Bands Observed in Impact-Induced Luminescence, J. Geophys. Res., 108(E12), 5140.
[8] Sugita, S., Schultz, P. H., 1998, Spectroscopic measurements of vapor clouds due to oblique impacts, Journal of Geophysical Research, Vol. 103, No. E8, pp. 19,427–19,441.
[9] Lawrence, R. J., Chhabildas, L. C., Reinhart, W. D., 2006, Impact Flash Spectroscopy at Impact Velocities Approaching 20 km/s, 57th Aeroballistics Range Association.
[10] Reinhart, W. D., Chhabildas, L. C., Thornhill, T. F., Lawrence, R. J., 2006, Spectral Measurements of Hypervelocity Impact Flash, International Journal of Impact Engineering, Volume 33, Issues 1–12, pp. 663–674.
[11] Tsemblis K., Burchell M.J., Cole M.J., Margaritis N., Residual temperature Measurements of light flash under hypervelocity impact, International Journal of Impact Engineering, 35 (11). pp. 1368-1373.
[12] J. Osterholz, F. Brandl, M. Cerchez, T. Fischer, D. Hemmers, B. Hidding, A. Pipahl, G. Pretzler, S. Rose, and O. Willi, 2008, Extreme ultraviolet emission from dense plasmas generated with sub-10-fs laser pulses, Phys. Plasmas 15, 103301.
[13] Sakka, T., Nakajima, T., Ogata, Y., 2002, Spatial Population Distribution of Laser Ablation Species Determined by Self-Reversed Emission Line Profile, Journal of Applied Physics, Vol. 92, No. 5, pp. 2296–2303.

[14] Pakhal, H., 2008, Spectral Measurements of Incipient Plasma Temperature and Electron Number Density during LASER Ablation of Aluminum in Air, Appl. Phys. B 90, pp. 15–27.
[15] Liu, H. C., Mao, X. L., 1999, Early Phase Laser Induced Plasma Diagnostics and Mass Removal during Single-Pulse Laser Ablation of Silicon, Spectrochim Acta Part B 54, pp. 1607–1624.
[16] Bastiaans, G., 1985, The Calculation of Electron Density and Temperature in Ar Spectroscopic Plasmas from Continuum and Line Spectra, Spectrochim Acta, Vol. 40B, No. 7, pp. 885–892.
[17] Schulz-von der Gathen, V., 2010, Plasmadiagnostik (lecture notes), Ruhr-Universität Bochum.
[18] Atomic and Molecular Data Services, About FLYCHK, [Online 2.4.2012], http://www-amdis.iaea.org/FLYCHK/ZBAR/index.php.
[19] Wiese, W., 1990, Experimental Stark Widths and Shifts for Spectral Lines of Neutral and Ionized Atoms, J. Phys. Chem. Ref. Data, Vol. 19, No. 6, pp. 1307–1385.
[20] Tamaki, S., Kuroda ,T., 1987, The Electronic Partition Functions of Atoms and Ions between 7000 and 12000 K, Spectrochimica Acta Part B: Atomic Spectroscopy, Volume 42, Issue 10, pp. 1105–1111.
[21] Brussard P., van de Hulst H., Approximation Formulas for Nonrelativistic Bremsstrahlung and Average Gaunt Factors fo a Maxwellian Electron Gas, 1962, Review of Modern Physics, Vol 34,Number 3, pp. 507–520.

Appendix A.

Table 1. Parameters for the one dimensional radiative transfer model.

Symbol	Definition	Value	Unit	Method of evaluation
T	temperature	32,000	K	adjusted
N_{e0}	electorn density parameter	$1*10^{19}$	cm^{-3}	adjusted
N_{1a}	population parameter $^2P_{3/2}$ level 394.4 nm	$1*10^{18}$	cm^{-3}	adjusted
N_{1b}	population parameter $^2P_{1/2}$ level 396.1 nm	$0.5*10^{18}$	cm^{-3}	calculated
N_2	population parameter exited state $^2S_{1/2}$	$2.5*10^{15}$	cm^{-3}	calculated
σ	distribution parameter electrons	$2.0*10^{-3}$	m	estimated
σ_1	distribution parameter ground state	$2.7*10^{-3}$	m	estimated
σ_2	distribution parameter excited state	$2.0*10^{-3}$	m	estimated
g_a	degeneracy $^2P_{3/2}$ level 394,4 nm	4	-	[18]
g_b	degeneracy $^2P_{1/2}$ level 396,1 nm	2	-	[18]
g_2	degeneracy $^2S_{1/2}$ level	2	-	[18]
A_{21a}	Einstein coefficient for spontaneous emission 394.4 nm $^2P_{3/2}$	$9.8*10^{7}$	s^{-1}	[18]
A_{21b}	Einstein coefficient for spontaneous emission 396.1 nm $^2P_{1/2}$	$4.91*10^{7}$	s^{-1}	[18]
v_{0a}	frequency 394.4 nm $^2P_{3/2}$	$7.581*10^{14}$	s^{-1}	[18]
v_{0b}	frequency 396.1 nm $^2P_{1/2}$	$7.548*10^{14}$	s^{-1}	[18]
w	Stark broadening parameter	$4.22*10^{14}$	nm/m^{-3}	[19]
d	Stark shift parameter	$2.42*10^{14}$	nm/m^{-3}	[19]
x	size of plasma plume	$4*10^{-2}$	m	measured

Appendix B.

Table 2. Parameters for the line to continuum temperature determination.

Symbol	Definition	Value	Unit	Reference
ε_l	line emission coefficient	from fitted spectrum	-	-
ε_c	continuum emission coefficient	from fitted spectrum	-	-
E_i	Ionization energy	$9.57*10^{-19}$	J	[18]
E_2	energy excited state	$5.03*10^{-19}$	J	[18]
λ_l	wavelength transition	$3.944*10^{-7}$	m	[18]
λ_c	wavelength transition	$3.944*10^{-7}$	m	-
g_2	degeneracy excited state	2	-	[18]
C	summarized constants	$2.01*10^{-5}$	sK	[16]
A_{21}	Einstein coefficient spontaneous emission 394.4 nm $^2P_{3/2}$	$9.8*10^{7}$	s^{-1}	[18]
U	partition function ion	7.6	-	[20]
ξ	free-bound factor	0.4	-	[21]
h	Planck constant	$6.63*10^{-34}$	Js	[18]
k	Boltzmann constant	$1.38*10^{-24}$	J/K	[18]